Electronic Supplemental Information

Study of Proximity coupled magnetic anisotropy in V doped SnTe using Spin Resonance and Magnetic Measurement

Subhadip Ghosh† and Sanjeev Kumar Srivastava‡
†School of Nano Science and Technology Indian Institute of Technology, Kharagpur, 721302
‡Department of Physics, Indian Institute of Technology, Kharagpur, 721302

I. XPS Valence Band Spectra:

Figures S2 (c)-(e) show the Al Kα valence band photoemission (PE) spectra for bare SnTe, and $V_xSn_{1-x}Te$ (x=0.03, and 0.08) V-doped SnTe QDs, respectively. The data have been corrected for an integrated Shirley and noisy background [1]. The obtained XPS valence band spectra can be divided into three regions:- 6eV to -2eV, -2eV to 3eV, and 3eV to 12eV. The intensity of XPS valence band spectra is directly proportional to the occupation of the electron. The occupation in the region -6eV to -2eV is very small, which signifies that all synthesized composites are in the semiconducting region. In the second region (-2eV to 3eV), there is a sudden change in occupation, revealing that the valence band is started from this region. The intersection of the 1st and 2nd region slop gives the VBM (Valence band maxima) position of the nano-composite. The VBM position of bare SnTe, and VxSn1−xTe (x=0.03, and 0.08) V-doped SnTe are -1.43eV, -1.21eV, -1.08eV respectively. This signifies that the valence band maxima shifts towards the Fermi level as V acts as a donor impurity. Incorporating V increases the overall defect concentration, increasing the band gap and shifting the conduction band maxima away toward the Fermi level. The above result is consistent with the band gap increase from the Tauc plot from FTIR spectra. The valence band of SnTe consists of Te 5p orbital and localized d electron of vanadium. That's why the slope in the 2nd region for the V-doped system is steeper than that of bare SnTe. This proves that there is a localized d electron (either in V +2 or in V +4 state), which modulates the valence band of SnTe. In the reference [2], the V2O3 and VO2 show a peak close to the fermi level, as the small size and high electronegativity makes the hybridization among O 2p orbital with the V 3d orbital, considerably weaker. But in our case, the large size and smaller electronegativity make the polarizability and covalency of Te maximum among all chalcogenides. That's why the hybridization among the 5p orbital of Te with the 3d orbital of V is considerably stronger. The third region (3eV to 14eV) peaks near 5.5eV, consisting of Te 5p electron. Hence, the above observation is consistent with the expected modulation of the energy band structure in the presence of defect states (Sn vacancy) and Vanadium (V) impurity.

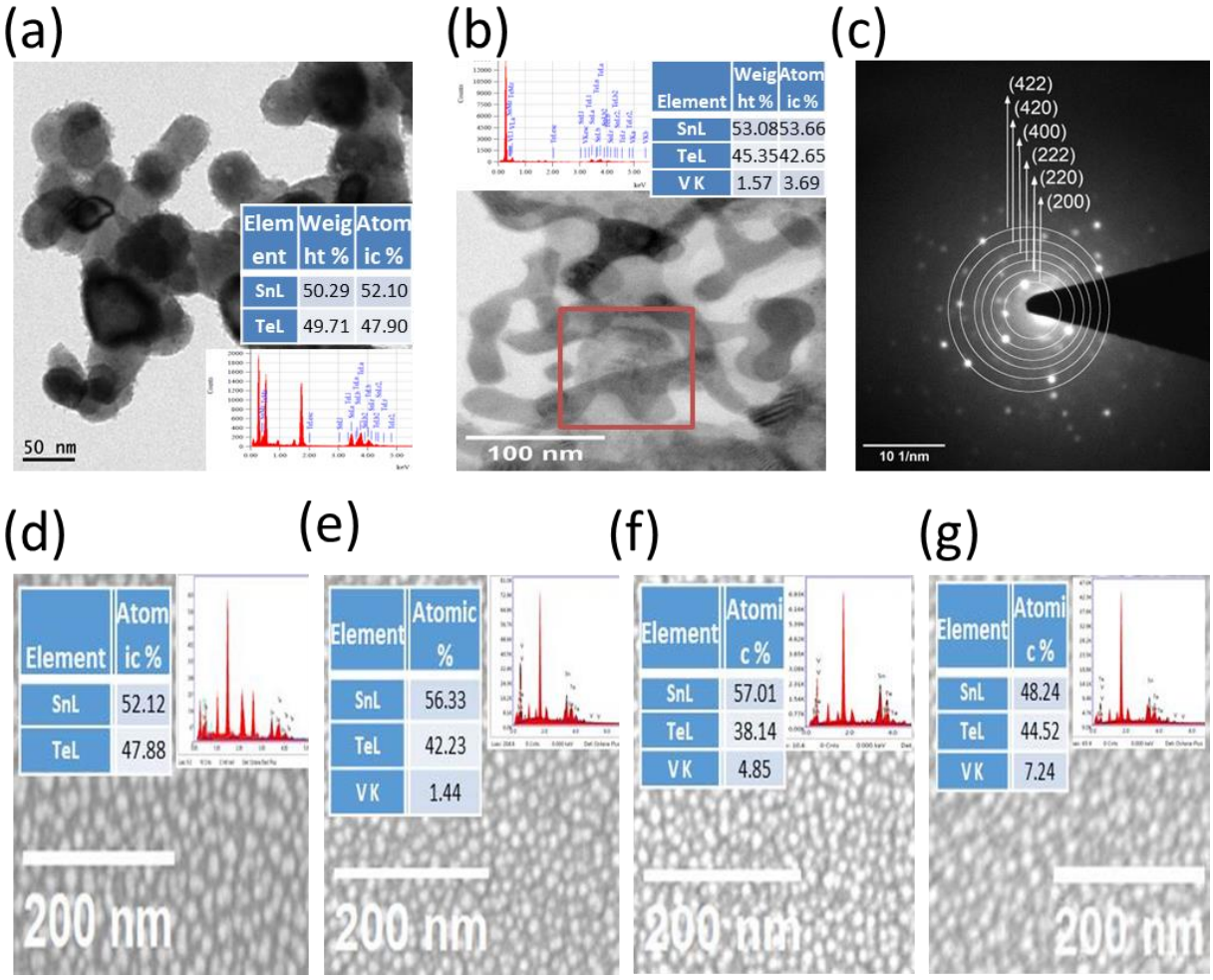

FIG. S1. HRTEM image and the corresponding EDX data of (a) bare SnTe, and (b) $V_{0.03}Sn_{0.97}Te$. (c) SAED pattern of bare SnTe. FEGSEM image and the corresponding EDX data of (d) SnTe, (e) $V_{0.03}Sn_{0.97}Te$, (f) $V_{0.05}Sn_{0.95}Te$, and (g) V0.08Sn0.92Te.

.

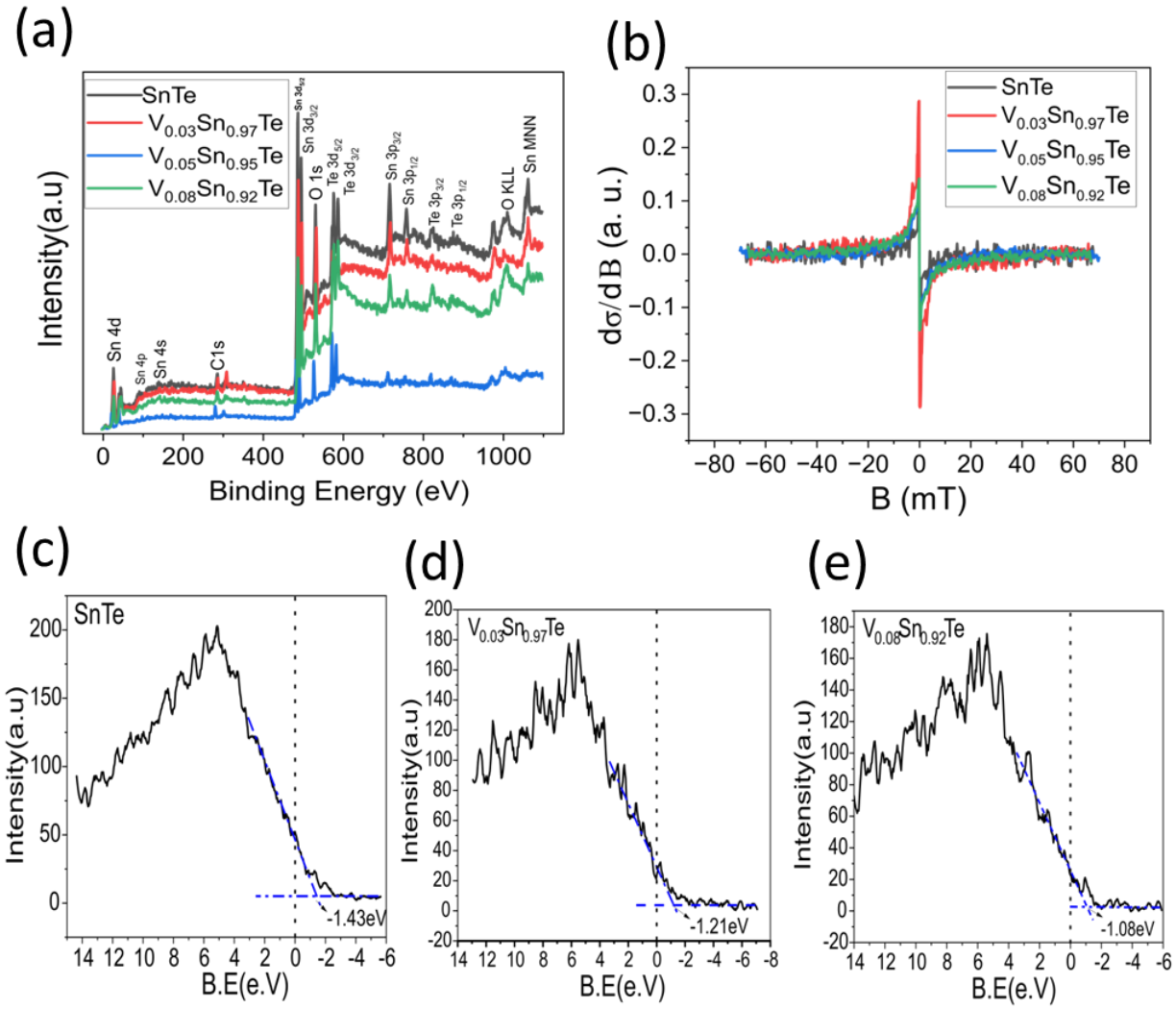

FIG. S2. (a) XPS survey spectra of SnTe, and VxSn1−xTe (x=0.03, 0.05, 0.08) V-doped SnTe, (b) Comparison of Low temperature (14 K) ESR differential conductivity of SnTe, and $V_xSn_{1-x}Te$ (x=0.03, 0.05, 0.08) V-doped SnTe. . XPS valence band spectra of (c) Bare SaTe, (d) 3% V-doped SnTe, and (e) 8% percent V-doped SnTe.

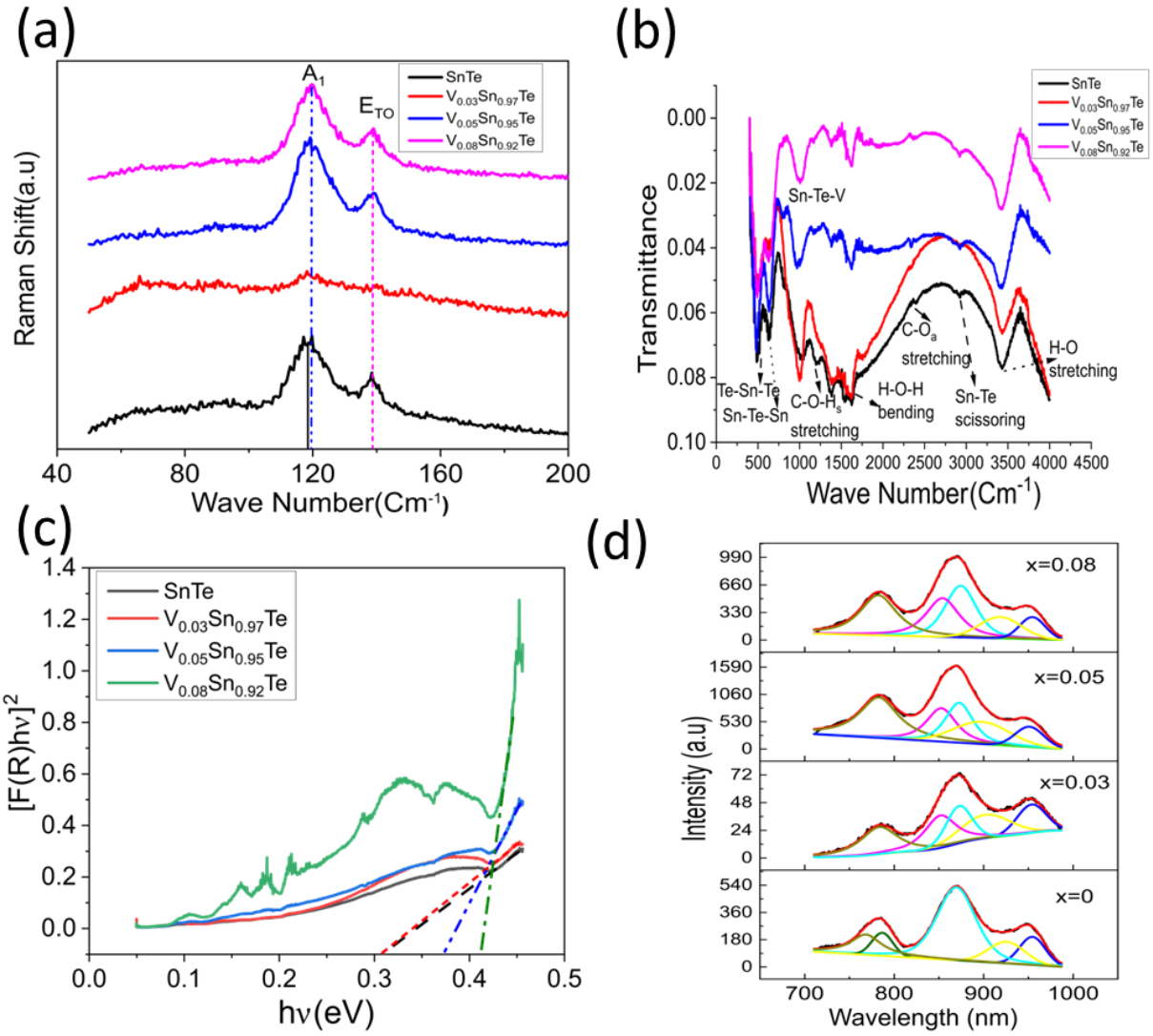

FIG. S3. (a) Raman Spectra, (b) FTIR Spectra and (c) Tauc plot of pristine and $V_xSn_{1-x}Te$ (x=0.03, 0.05, 0.08) V-doped SnTe from FTIR absorption, (d) Photoluminescence spectra of bare and $V_xSn_{1-x}Te$ (x=0.03, 0.05, 0.08) V-doped SnTe.

TABLE SI The integrated charge content of Sn 3d and 4d orbital with and without SOC within the valence band up to -5 eV of SnTe, Snv Te, VSnTe, VSnv Te, vSnTe, and vSnv Te.

Composition Symbol	Charge (a.u)
$SnTe_{3d-Sn}$	0.00558
Sn_vTe_{3d-Sn}	0.004280
$VSnTe_{3d-Sn}$	0.00758
$VSn_v\ Te_{3d-Sn}$	0.007101
$vSnTe_{3d-Sn}$	0.01814
$vSn_v\ Te_{3d-Sn}$	0.006542
$SnTe_{3d-Sn}^{soc}$	0.00546
$Sn_v\ Te_{3d-Sn}^{soc}$	0.00506
$VSnTe_{3d-Sn}^{soc}$	0.007423
$VSn_v\ Te_{3d-Sn}^{soc}$	0.0704
$vSnTe_{3d-Sn}^{soc}$	0.006385
$vSn_v\ Te_{3d-Sn}^{soc}$	0.002452
$SnTe_{4d-Sn}^{soc}$	0.00219
$Sn_v\ Te_{4d-Sn}^{soc}$	0.00204
$VSnTe_{4d-Sn}^{soc}$	0.004805
$VSn_v\ Te_{4d-Sn}^{soc}$	0.00422
$vSnTe_{4d-Sn}^{soc}$	0.0109
$vSn_v\ Te_{4d-Sn}^{soc}$	0.004318

TABLE SII The integrated charge content of V 4d and 5d orbital with and without SOC, within the valence band up to -5 eV of VSnTe, VSn_vTe, vSnTe, and vSn_vTe.

Composition Symbol	Charge (a.u)
$VSnTe_{4d-V}$	4.19
$VSn_v\ Te_{4d-V}$	3.71
$vSnTe_{4d-V}$	4.14217
$vSn_v\ Te_{4d-V}$	3.70465
$VSnTe_{4d-V}^{soc}$	1.63
$VSn_v\ Te_{4d-V}^{soc}$	1.56
$VSn_v\ Te_{4d-V}^{soc}$	2.32
$VSn_v\ Te_{5d-V}^{soc}$	2.31
$vSnTe_{4d-V}^{soc}$	1.6093
$vSn_v\ Te_{4d-V}^{soc}$	1.521
$vSnTe_{5d-V}^{soc}$	2.2516
$vSn_v\ Te_{5d-V}^{soc}$	2.1858

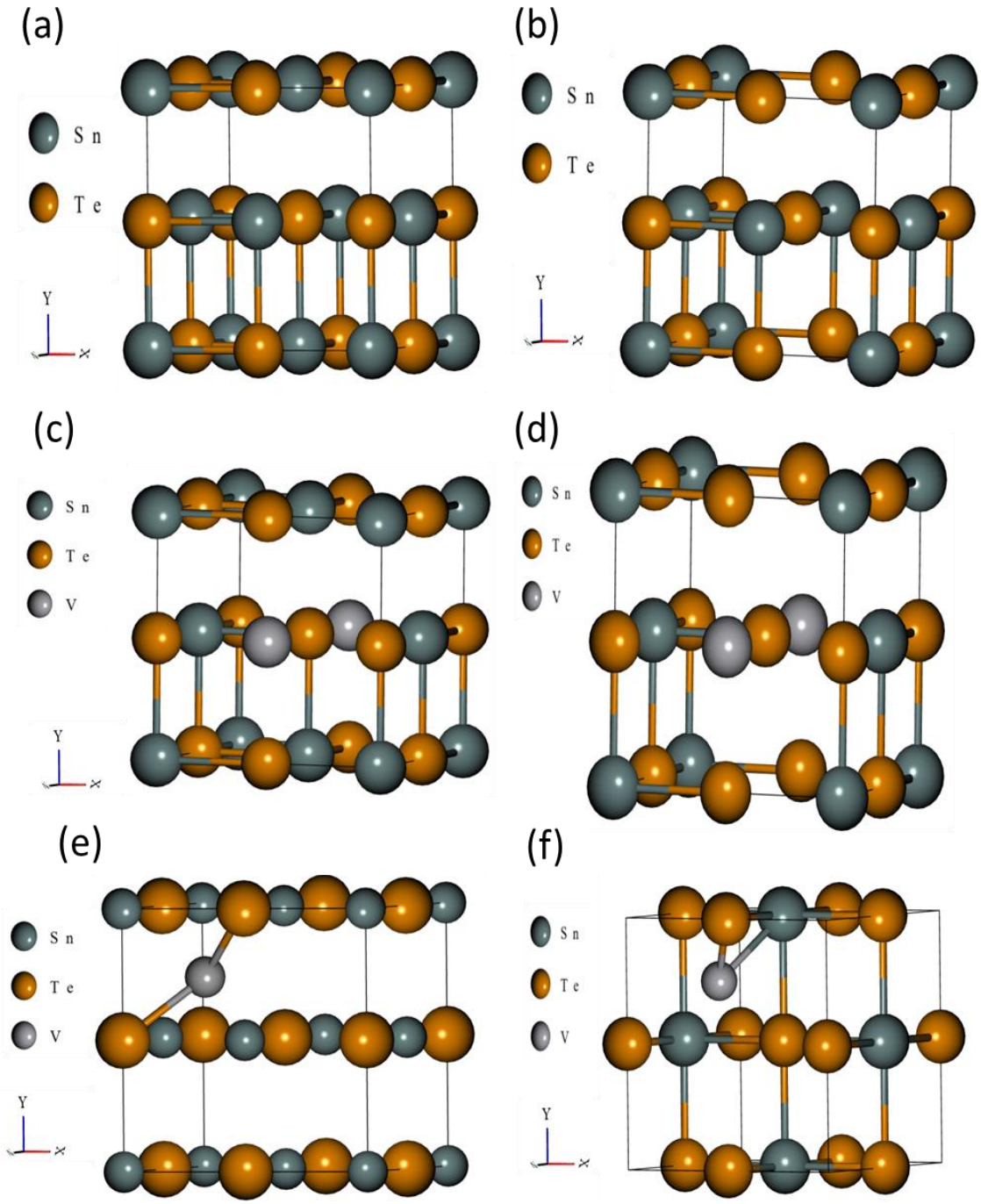

FIG. S4. FCC structure with Fm-3m space group of (a) SnTe, (b) SnTe with Sn vacancy (c) V doped SnTe, (d) V doped SnTe with Sn vacancy, (e) Interstitial V doped SnTe, and (f) Interstitial V doped SnTe with Sn vacancy.

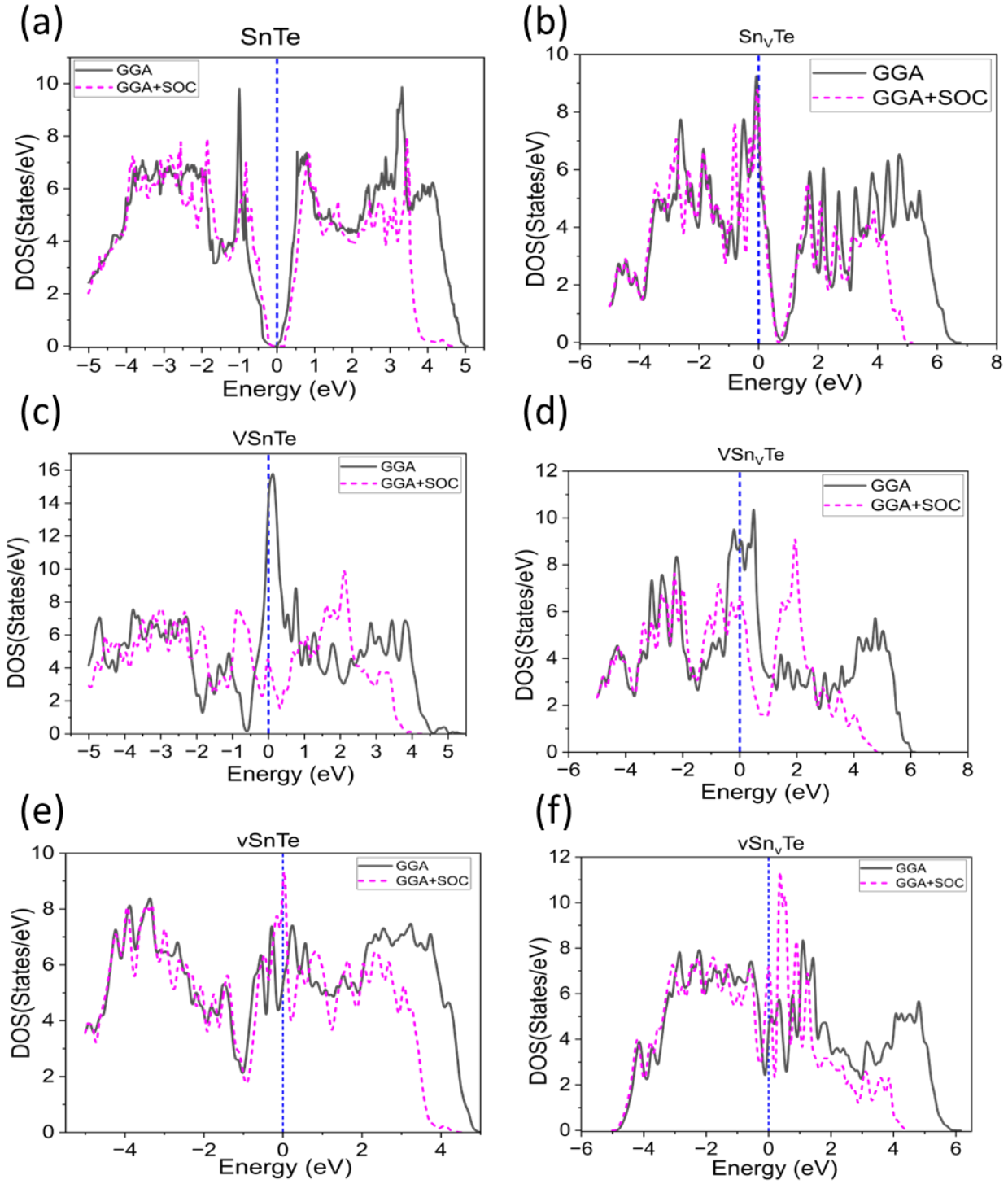

FIG. S5 DOS with GGA and GGA+SOC of (a) SnTe (b) SnTe with Sn vacancy (Sn_VTe), (c) V-doped SnTe (VSnTe), (d) V-doped SnTe with Sn vacancy (VSn_VTe), (e) SnTe with interstitial V (vSnTe), and (f) SnTe with Sn vacancy and interstitial V (vSn_vTe).

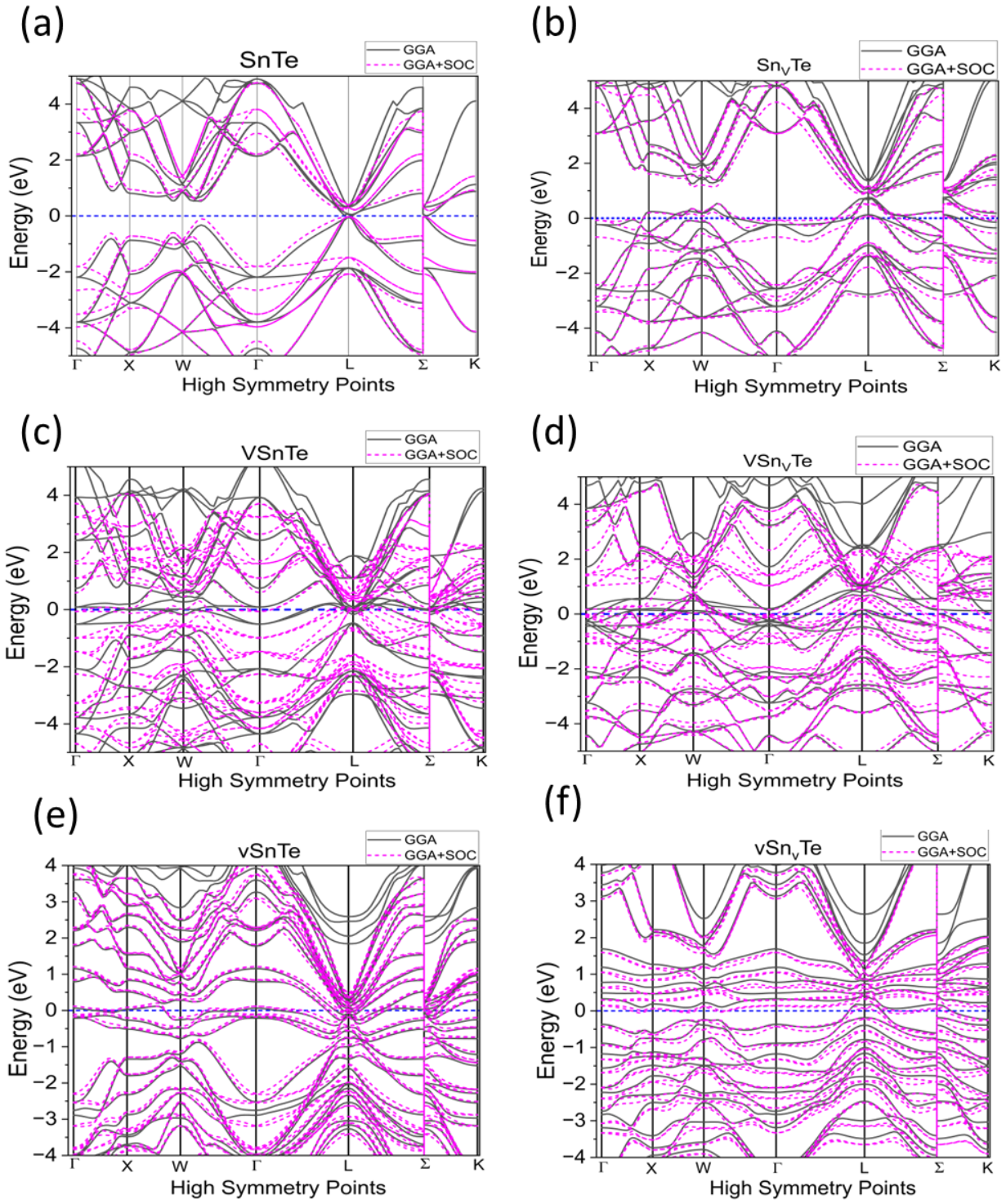

FIG. S6. Band Structure with GGA and GGA+SOC of (a) SnTe (b) Sn$_V$Te, (c) VSnTe, (d) VSn$_V$Te, (e) vSnTe, and (f) vSn$_V$Te.

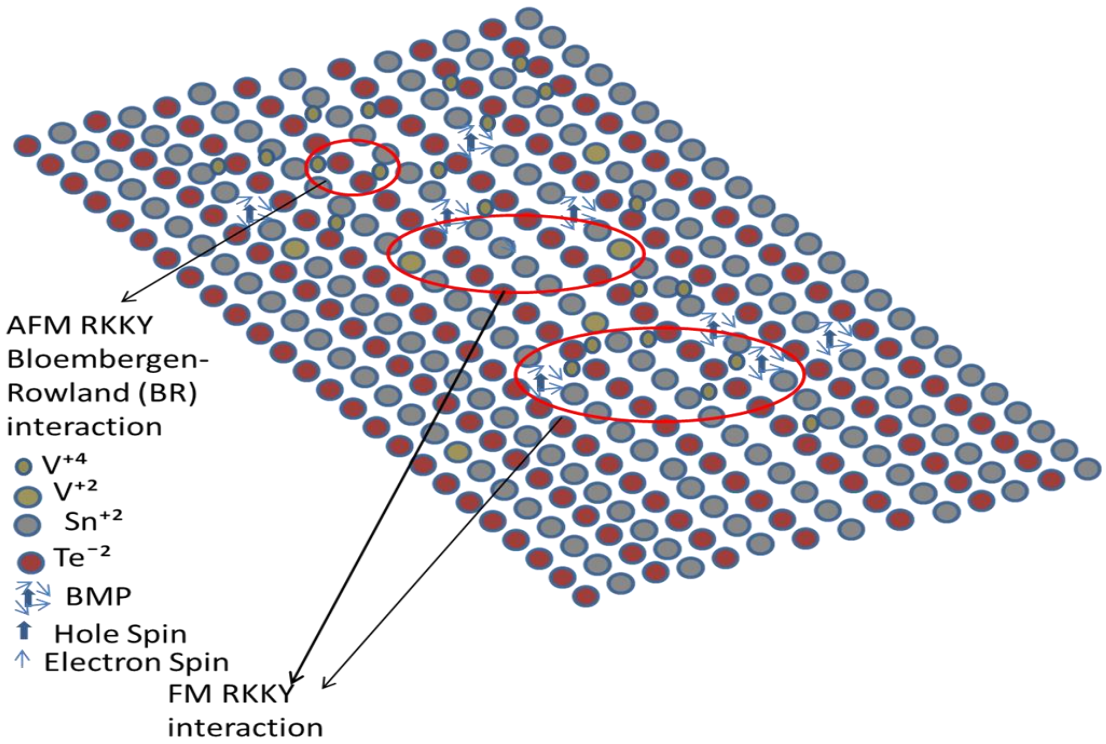

FIG. S7. Schematic of SnTe with interstitial (V+4) and substitutional (V+2) impurity and BMP showing FM and AFM (Bloembergen-Rowland (BR)) RKKY exchange interaction.

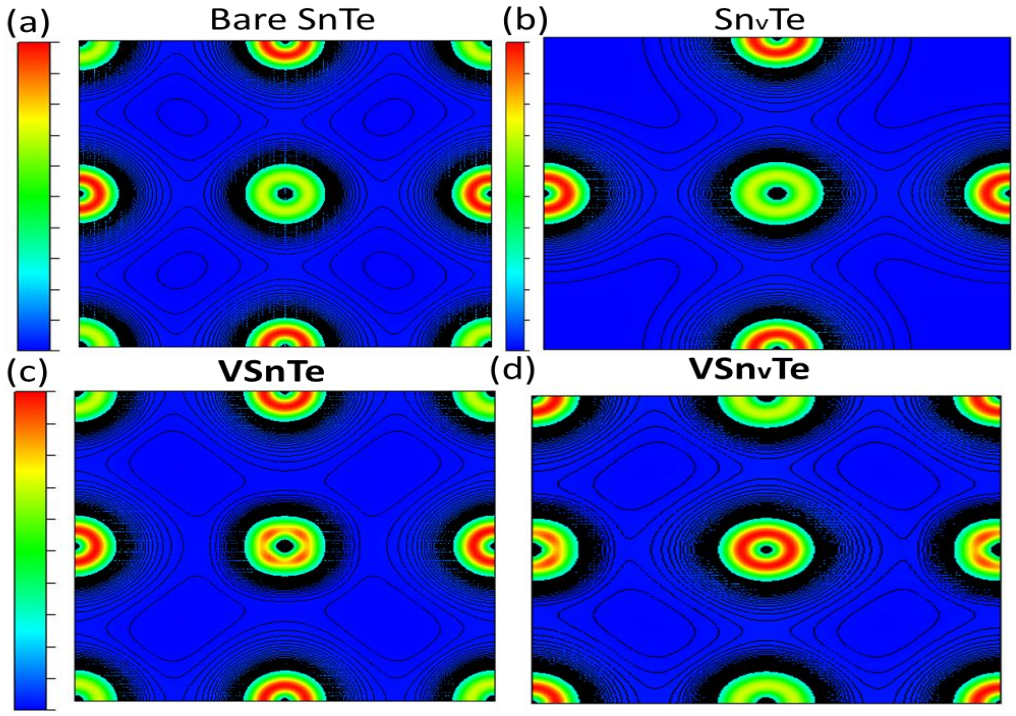

FIG.S8. Comparison of 2D electron density contour map of (a) SnTe, (b) Sn_VTe, (c) VSnTe, and (d) VSn_VTe.

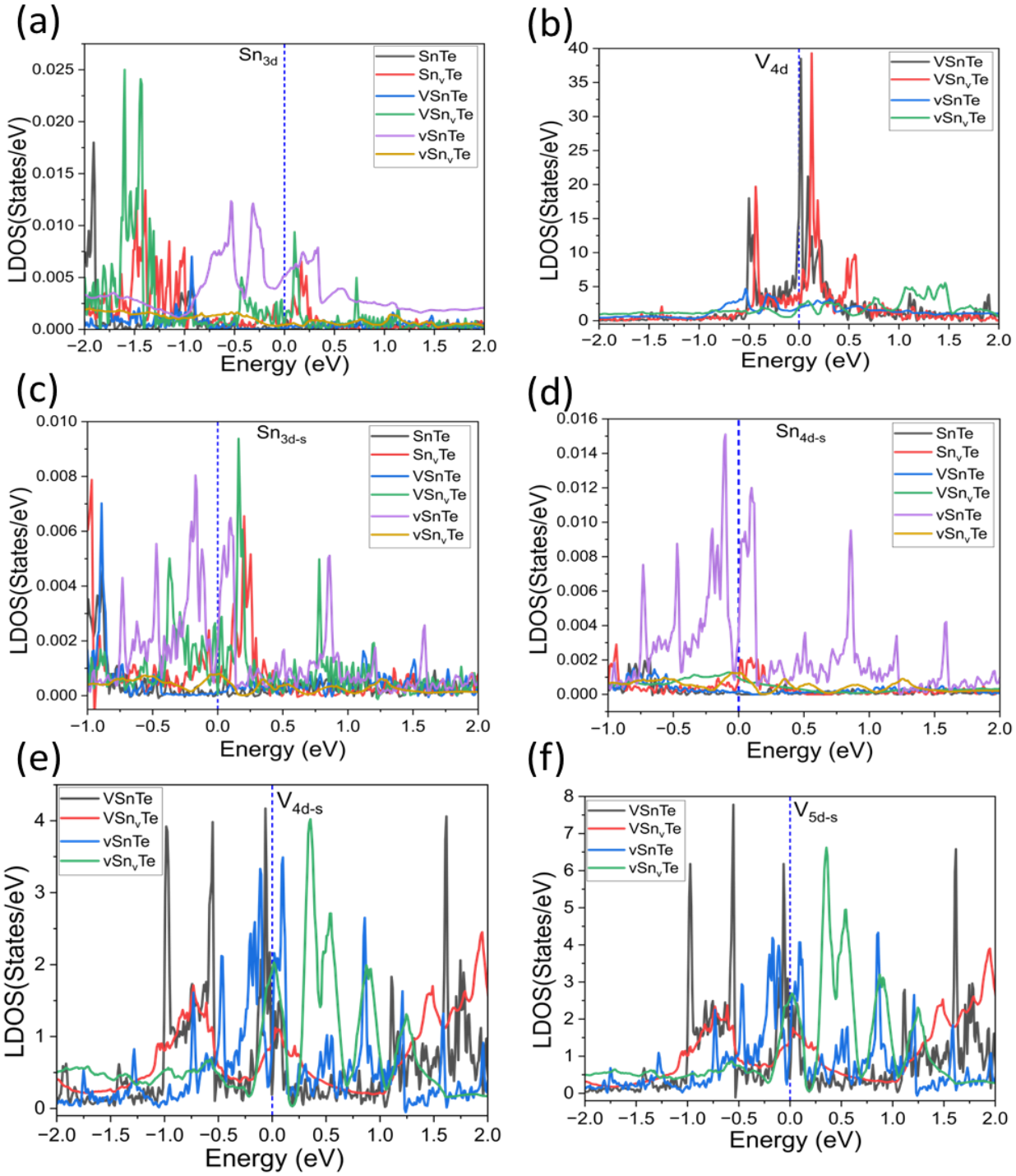

FIG. S9. Comparison of the local density of states of (a) Sn 3d orbitals of SnTe, SnV Te, VSnTe, VSnV Te, vSnTe, and vSnv Te and (b) V 4d orbital of VSnTe, VSnV Te, vSnTe, and vSnv Te without SOC, respectively. Comparison of the local density of states of (c) Sn 4d, and (d) Sn 5d, orbitals of SnTe, SnV Te, VSnTe, VSnV Te, vSnTe, and vSnv Te and (e) V 5d, and (f) V 6d orbitals of VSnTe, VSnV Te, vSnTe, and vSnv Te, with SOC, respectively.

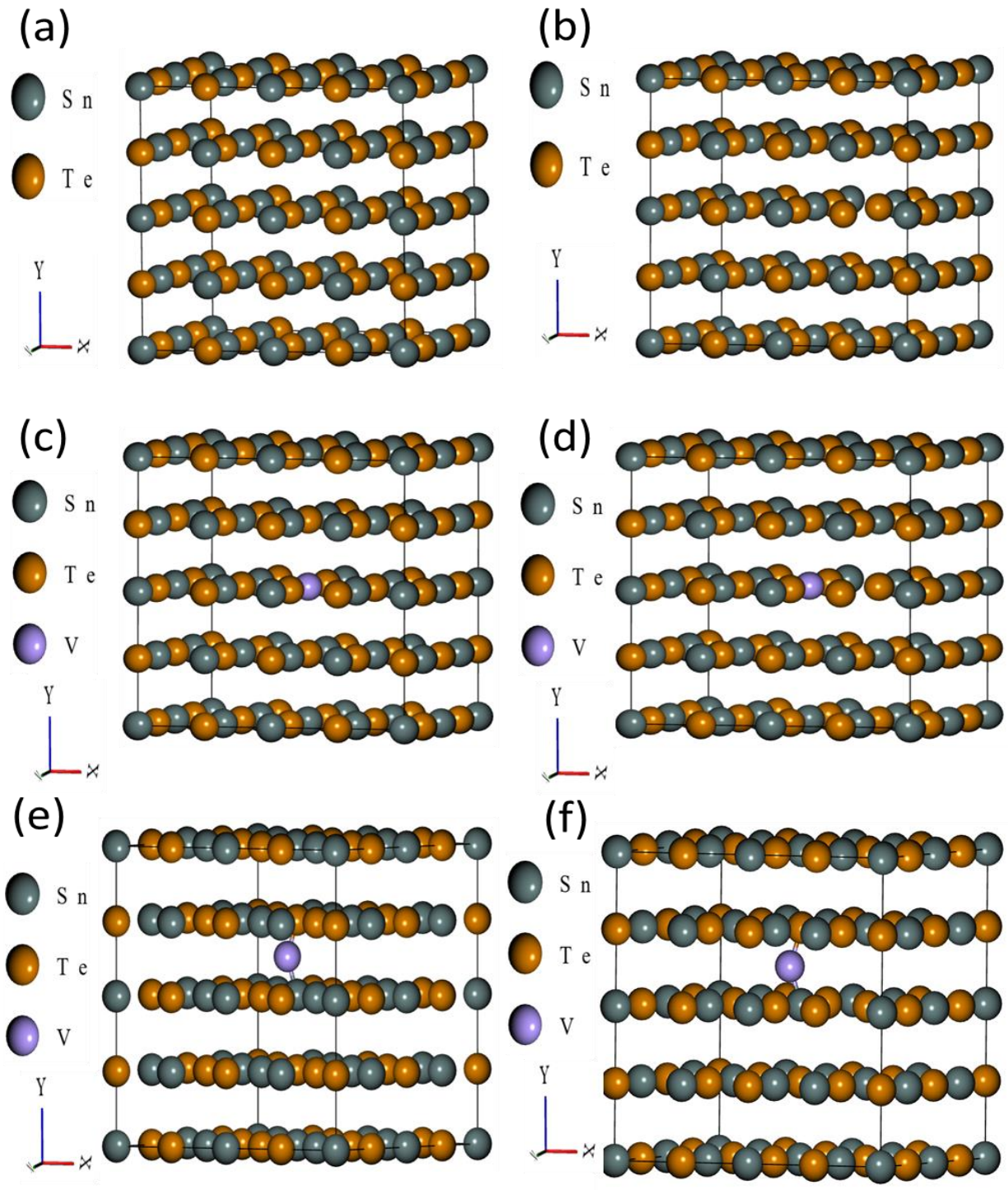

FIG. S10. 2X2X2 supercell with Fm-3m space group of (a) SnTe, (b) SnTe with Sn vacancy (c) V doped SnTe, (d) V doped SnTe with Sn vacancy, (e) Interstitial V doped SnTe, and (f) Interstitial V doped SnTe with Sn vacancy.

TABLE SIII The integrated charge content of Sn 3d and 4d orbital with and without SOC within the valence band up to -5 eV of SnTe, Snv Te, VSnTe, VSnv Te, vSnTe, and vSnv Te in 2x2x2 supercell.

Composition Symbol	Charge (a.u)
$SnTe_{3d-Sn}$	0.0078
Sn_vTe_{3d-Sn}	0.00417
$VSnTe_{3d-Sn}$	0.00572
$VSn_v\ Te_{3d-Sn}$	0.004227
$vSnTe_{3d-Sn}$	0.0082
$vSn_v\ Te_{3d-Sn}$	0.00812
$SnTe_{3d-Sn}^{soc}$	0.004701
$Sn_v\ Te_{3d-Sn}^{soc}$	0.003182
$VSnTe_{3d-Sn}^{soc}$	0.005724
$VSn_v\ Te_{3d-Sn}^{soc}$	0.003553
$vSnTe_{3d-Sn}^{soc}$	0.006708
$vSn_v\ Te_{3d-Sn}^{soc}$	0.006204
$SnTe_{4d-Sn}^{soc}$	0.005447
$Sn_v\ Te_{4d-Sn}^{soc}$	0.004611
$VSnTe_{4d-Sn}^{soc}$	0.006795
$VSn_v\ Te_{4d-Sn}^{soc}$	0.00436
$vSnTe_{4d-Sn}^{soc}$	0.007506
$vSn_v\ Te_{4d-Sn}^{soc}$	0.007129

TABLE SIV The integrated charge content of V 4d and 5d orbital with and without SOC, within the valence band up to -5 eV of VSnTe, VSn_vTe, vSnTe, and vSn_vTe in 2x2x2 supercell.

Composition Symbol	Charge (a.u)
$VSnTe_{4d-V}$	3.43
$VSn_v\ Te_{4d-V}$	3.25
$vSnTe_{4d-V}$	3.12
$vSn_v\ Te_{4d-V}$	2.98
$VSnTe_{4d-V}^{soc}$	1.6993
$VSn_v\ Te_{4d-V}^{soc}$	1.6225
$vSn_v\ Te_{4d-V}^{soc}$	1.63036
$vSn_v\ Te_{4d-V}^{soc}$	1.5296
$VSnTe_{5d-V}^{soc}$	2.3234
$VSn_v\ Te_{5d-V}^{soc}$	2.2601
$vSnTe_{5d-V}^{soc}$	2.2163
$vSn_v\ Te_{5d-V}^{soc}$	2.1858

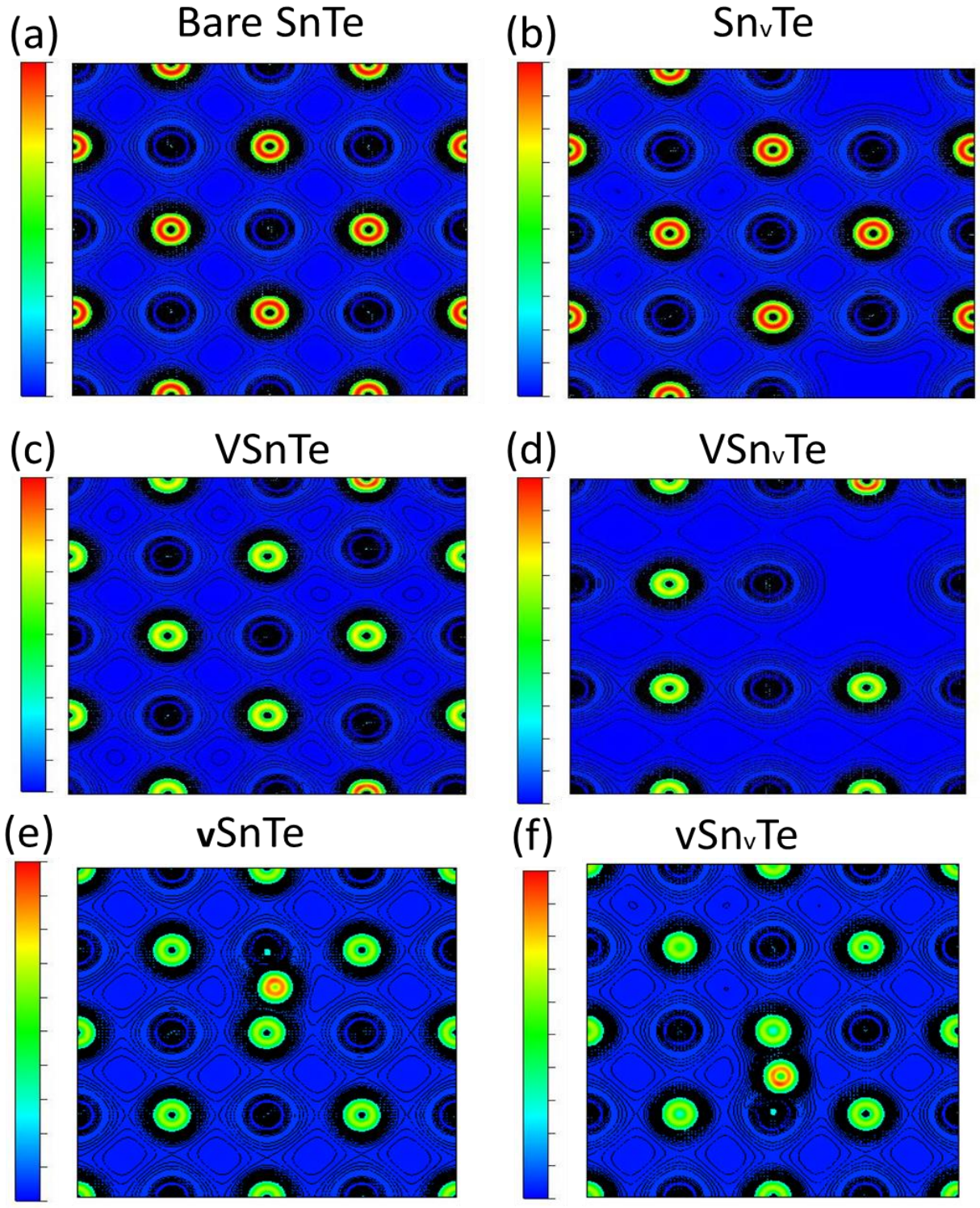

FIG.S11. Comparison of 2D electron density contour map of (a) SnTe, (b) Sn_VTe, (c) VSnTe, (d) VSn_VTe (e) vSnTe, and (f) vSn_VTe in 2x2x2 supercell structure.

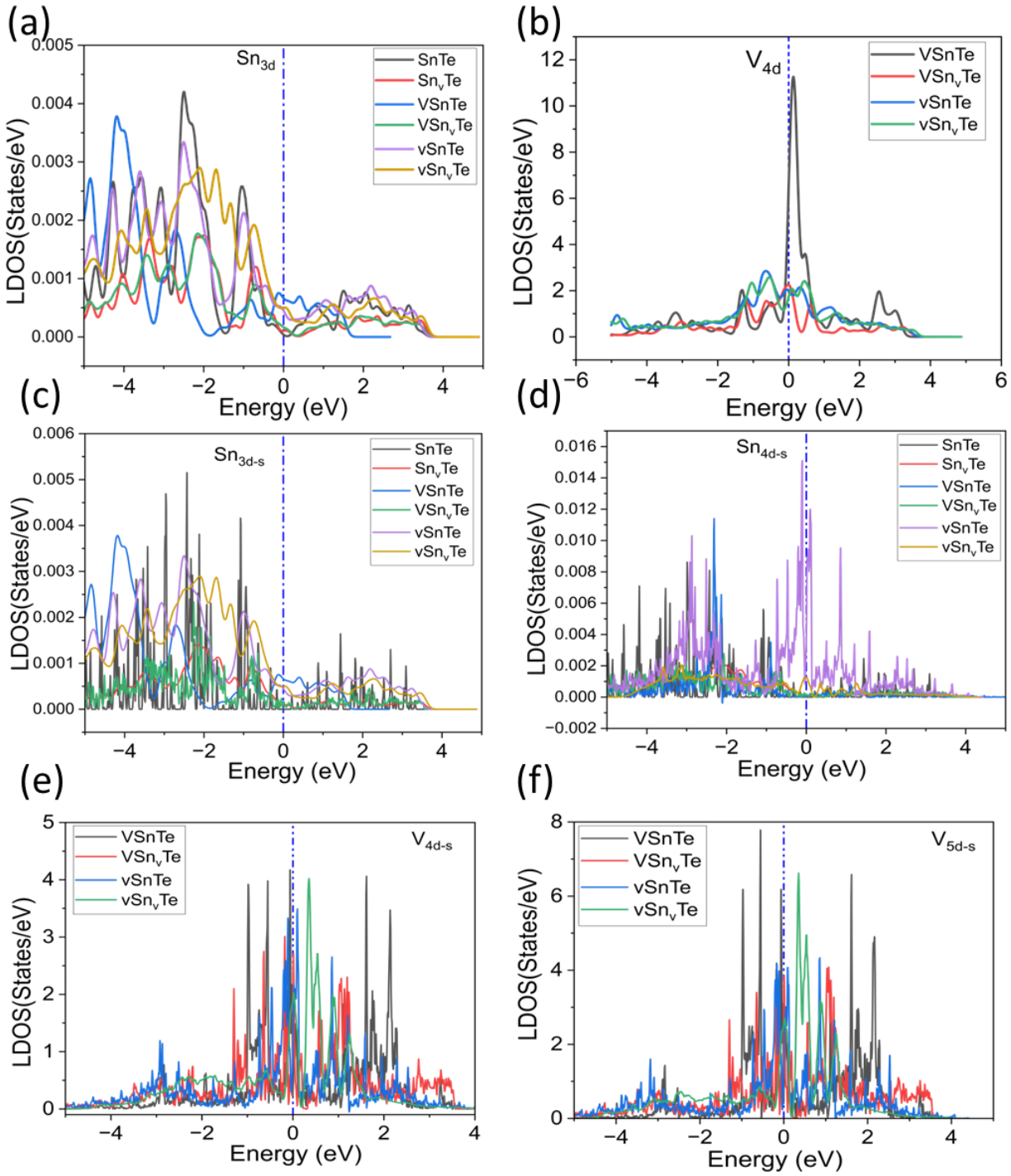

FIG. S12. Comparison of the local density of states of (a) Sn 3d orbitals of SnTe, SnV Te, VSnTe, VSnV Te, vSnTe, and vSnv Te and (b) V 4d orbital of VSnTe, VSnV Te, vSnTe, and vSnv Te without SOC, respectively. Comparison of the local density of states of (c) Sn 4d, and (d) Sn 5d, orbitals of SnTe, SnV Te, VSnTe, VSnV Te, vSnTe, and vSnv Te and (e) V 5d, and (f) V 6d orbitals of VSnTe, VSnV Te, vSnTe, and vSnv Te, with SOC, respectively in 2x2x2 supercell structure.

References:-

[1] V. Ivanshin, V. Yushankhai, J. Sichelschmidt, D. Zakharov, E. Kaul, and C. Geibel, Esr study of the anisotropic exchange in the quasi-one-dimensional antiferromagnet Sr_2 V_3O_9, Physical Review B 68, 064404 (2003).
[2] R. Zimmermann, R. Claessen, F. Reinert, P. Steiner, and S. H¨ufner, Strong hybridization in vanadium oxides: evidence from photoemission and absorption spectroscopy, Journal of Physics: Condensed Matter 10, 5697 (1998).